Supplementary Materials for

The Shortest-Known–Period Star Orbiting Our Galaxy's Supermassive Black Hole

L. Meyer, A. M. Ghez,* R. Schödel, S. Yelda, A. Boehle, J. R. Lu, T. Do, M. R. Morris, E. E. Becklin, K. Matthews

*To whom correspondence should be addressed. E-mail: ghez@astro.ucla.edu

This PDF file includes:

Materials and Methods
Supplementary Text
Figs. S1 and S2
Tables S1 to S5
References (*35–42*)

Materials and Methods

<u>Image</u> <u>construction</u>

Images are constructed from the speckle data sets by both shift-and-add (SAA), which has been our approach in the past (*37, 38, 7*), and Speckle holography, which is a new and more effective approach for this data set (*39*). In SAA, the images are registered based on the positions of the brightest speckle in the PSF of the short-exposure images (*40*). We implemented this approach similarly to past analyses of these data sets (*7, 37*), except for our use of a new distortion solution for NIRC (*35*). While the advantage of this approach is its computational efficiency as well as its robust treatment of edge-effects, the disadvantage is that information in all but the brightest speckle is not only lost but becomes a source of noise in a large, so-called "seeing-halo". To reduce the size of the seeing-halo, only frames with the minimum number of speckles are used. In spite of discarding photons, frame selection increases the overall dynamic range of the images because it is limited mainly by stellar crowding and the halos around the brighter stars. The images that went into the determination of S0-2's orbit have been constructed using SSA.

Speckle holography, on the other hand, is an image reconstruction method that makes use of the entire instantaneous PSF, or speckle cloud, of each speckle frame (*41, 42*). It constructs a best estimate of the object in the least squares sense and leads to images with higher dynamic range than SAA because it makes use of the entire speckle clouds. The main difficulty is an accurate extraction of the instantaneous PSF in the extremely crowded Galactic center star field. This is achieved via an iterative procedure and the use of multiple reference stars, as described by Schödel et al. (*39*). The images that went into the determination of S0-102's and S0-104's orbit have been constructed using Speckle holography.

The adaptive optics (AO) image reconstruction procedure for this study is similar to that used in the past for these data sets (*7, 14*). It differs only in that it corrects for differential atmospheric refraction and makes use of the new NIRC2 geometric optical distortion as reported by Yelda et al. (*35*).

<u>Source</u> <u>extraction</u> <u>and</u> <u>astrometry</u>

Sources are identified and characterized using the *StarFinder* software package (*18*), which iteratively carries out point spread function (PSF) fitting in crowded stellar fields and PSF modeling from the images being analyzed. Stars are identified by requiring that both their flux and their cross-correlation with the PSF lie above chosen thresholds that are user defined and that affect the number and reliability of sources identified in each image. In order to avoid false detections, we have taken a fairly conservative approach, which is similar to our previous work with a few exceptions that we describe here. In each image, we set the threshold for flux to be considered significant to 3σ above the noise, which is empirically estimated from comparing three sub-sets of the data. This empirical approach to noise estimation differs from our previous procedure and significantly reduces false detections associated with mismatches in the PSF. The treatment of the correlation threshold, which is a measure of how well a flux excess is in agreement with the PSF, is also different and is key to identifying S0-102, which is a faint source (with a K magnitude of ~17.3) in a very crowded region of the images.

Previously, the correlation threshold has been set independently of the type or quality of the data set at hand, i.e. it was not differentiated between Speckle, NGS-AO, and LGS-AO. Here, we treat different types of data sets separately. Data taken in LGS-AO mode are generally of the highest quality, and we therefore chose a correlation value of 0.5 for the average image ("deep image"), and a value of 0.3 for the three images consisting of a third of the data ("sub-set images"). For NGS-AO data as well as Speckle SSA data, we use a correlation value of 0.8 for the deep image and 0.6 for the sub-set images. Lastly, for Speckle holography a value of 0.7 for both the deep image and the sub-set images were chosen. Speckle holography leads to a structured background, which might be turned into apparent sources by *StarFinder*, and we therefore do not lower the correlation threshold in the sub-set images as we do in the other techniques to account for the lower signal-to-noise in the sub-set images.

The three sub-set images are used to grade the robustness of a source's detection in a given epoch. For the AO data sets, we consider a star to be a definite detection, if it gets also detected in at least two out of the three subset-images. The Speckle data have different noise properties so that a more conservative approach is advisable. We therefore only consider a source to be real if it gets detected in all three sub-set images. If a source detected in the epoch's complete data set does not pass these stringent sub-set image criteria, we discard it completely.

This approach along with the quality of the data set leads to average detection limits of 15.9, 17.0, 19.7 magnitudes for the Speckle shift-and-add, Speckle holography, and AO images. The limits for each epoch are provided in Table S2 and S3 for the Speckle and AO observations, respectively.

Three subset-images are also used to determine the error in the astrometry and photometry on the sources for each epoch. All epochs are aligned into a common reference frame following the description of Yelda et al.~(*35*). An additional alignment error is found by using a half sample bootstrap applied to the coordinate reference stars.

In order to search for stars with orbital periods that could be shorter than S0-2, who has a period of 16 years, we searched for stars whose detections are (1) all within a radius of ~0."25 (twice the semi-major axis of S0-2) of Sgr A*, the emissive source associated with the central black hole, and (2) describing a change of angle with respect to Sgr A* of more than 180 degrees. Three stars besides S0-2 satisfy these criteria. One of them (S0-103, named S19 in Gillessen et al.~(*8*)) is known to have a much longer period (~300 yrs), while the other two (S0-102 and S0-104) have no reported kinematic information beyond linear motion in the literature and are explored in this study.

The two stars are not detected in all epochs owing to the limited sensitivity of the Speckle and two early AO images -- S0-102 has a K magnitude of 17.3, S0-104 of 16.8 -- in addition to confusion with brighter sources. For S0-102, detection is prevented by overlap with S0-17 (S17 in (*8*)) between 2001 - 2003. The same happened in late 2008, and in 2011 with S0-103 (S19), and in early 2009 with Sgr A*/S0-104. S0-38 (S38) may have interfered with the 1998 - 1999 measurements. S0-104, which owing to the geometry of its orbit spends the years from 2002 - 2009 apparently close to Sgr A*, gets obstructed by S0-2, S0-17, Sgr A*, and possibly S0-38. Table S1 summarizes the resulting 13 measurements of the newly identified star S0-102.

Supplementary Text

The orbit of S0-2

Our current knowledge of the central gravitational potential is dominated by S0-2. Since we determine the orbital elements of S0-102 with fixed potential, we describe here S0-2's orbit and the parameter values of the central potential inferred from it.

We analyze S0-2's orbit within our standard astrometry approach (*7, 35*), which means using a high-correlation data set throughout (correlation thresholds set uniquely in StarFinder to 0.8 and 0.6 for the main image and the sub-set images), and shift-and-add Speckle data only. In addition to the radial velocities observed with Keck, we use all published values (*9*). Since the alignment of each epoch into a reference frame can be slightly different for different data sets, the inferred X_0, Y_0, X velocity, and Y velocity values (that describe the 2-dimensional position of the central mass at time 2000.0 and its velocity) can differ in different analyses. (In general, all inferred values can be different, however, the difference is statistically insignificant. In our case, the largest statistical difference is for X_0, which differs by only 1σ.) We therefore used X_0, Y_0, X velocity, and Y velocity from the low-correlation, Speckle holography analysis, and the other parameters of the central potential from the standard approach. We list the best-fit values in Table S4, and Fig. 2 and Fig. S2 depicts S0-2's orbit.
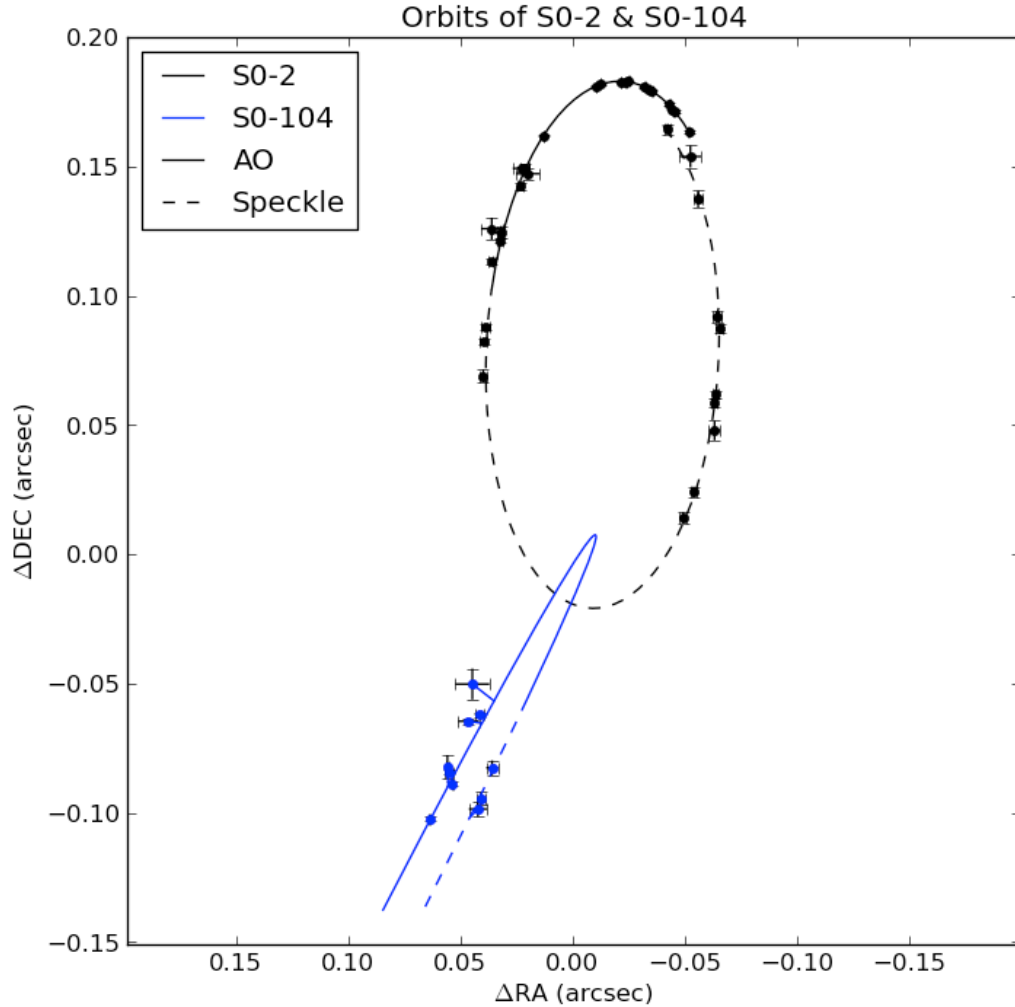
The orbit of S0-104

We present here the orbit of the newly detected star S0-104. This analysis uses the same data set and as the analysis for S0-102, i.e. low-correlation thresholds and Speckle holography. The latter is key in identifying S0-104's orbit. The orbital fit fixes the parameters of the central potential and infers the orbital elements with their uncertainties in the same way it was done for S0-102. Table S5 shows the values for S0-104's orbital elements, Fig. S2 depicts its orbit, which has a period of 80 years. S0-102 is therefore the only new star with an orbital period shorter than S0-2 (its orbital solution is described in the main body of this report).

Fig. S1.
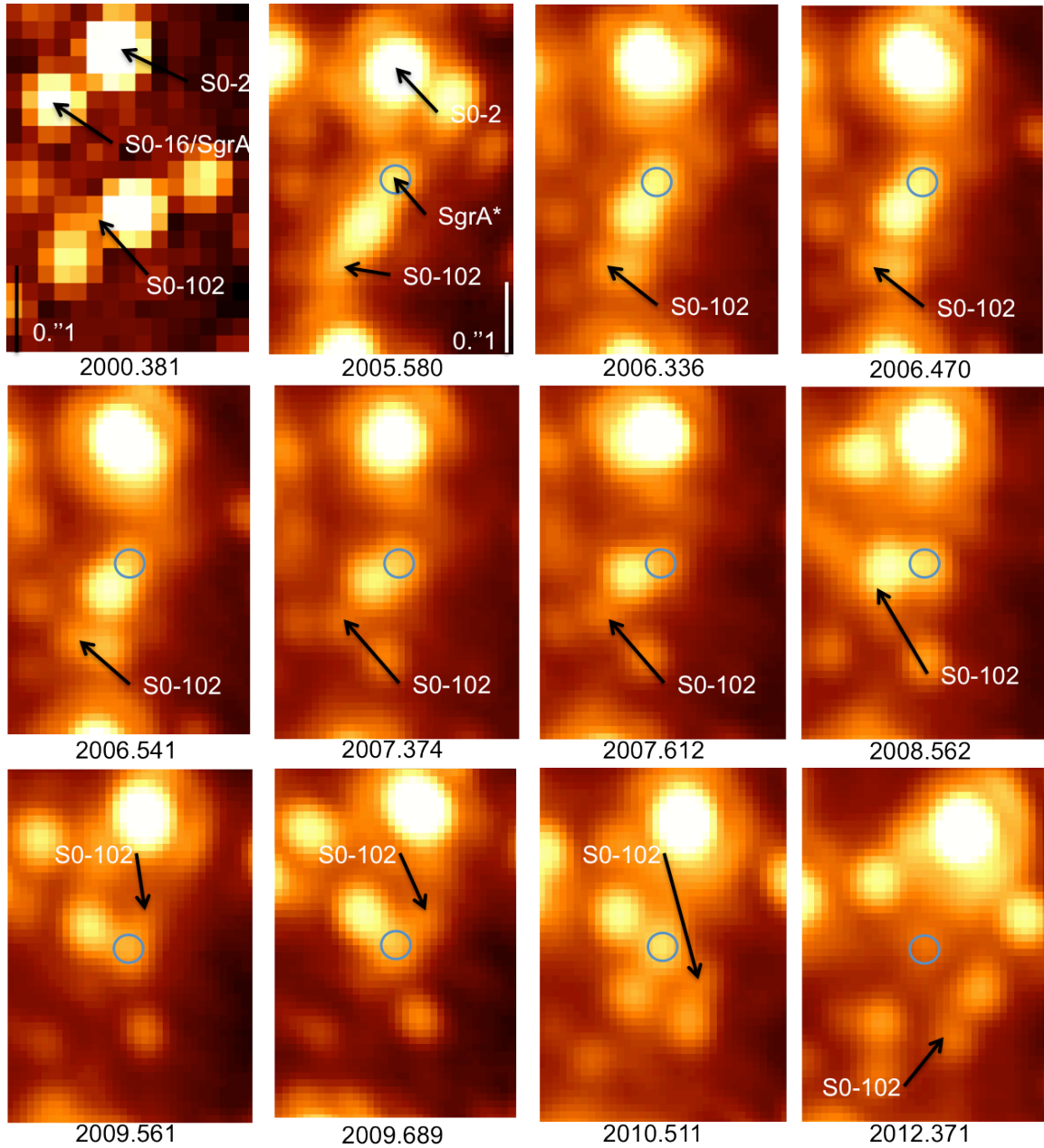
All detections of S0-102 (the detection in 2010.342 is shown in Fig. 1). The images are cleaned (pixel corrected, flat fielded, background subtracted) AO images with the exception of 2000.381, which is a Speckle holography reconstructed image. Each time the deep image of the epoch is shown. The blue circle marks Sgr A* in the AO images.

Fig. S2

The orbits of S0-2 (black) and S0-104 (blue). The data points and the best fits are shown. S0-2 orbits clockwise, S0-104 orbits counterclockwise. The dashed lines represent the part of the orbits that have been observed with Speckle data, the solid lines indicate AO observations. S0-104's detections range from 1999 to 2012, with astrometric data points in 1999-2001 and 2010-2012. The connecting lines to the best fit visualize the residuals. Note that while the best-fit orbits are not closing, the statistically allowed sets of orbital trajectories are consistent with a closed orbit. S0-104 has an orbital period of around 80 years.

Table S1.

Summary of S0-102 Measurements

Date (UT)	ΔRA (mas)	ΔDEC (mas)	Magnitude	Technique
2000.381	-55 $\pm$ 25	-123 $\pm$ 13	16.9 $\pm$ 0.2	Speckle
2005.580	75 $\pm$ 11	-145 $\pm$ 6	17.0 $\pm$ 0.8	AO
2006.336	77 $\pm$ 2	-126 $\pm$ 1	17.4 $\pm$ 0.1	AO
2006.470	76 $\pm$ 4	-124 $\pm$ 2	17.2 $\pm$ 0.1	AO
2006.541	77 $\pm$ 1	-121 $\pm$ 1	17.1 $\pm$ 0.1	AO
2007.374	81 $\pm$ 1	-87 $\pm$ 2	17.5 $\pm$ 0.2	AO
2007.612	78 $\pm$ 1	-75 $\pm$ 1	17.5 $\pm$ 0.1	AO
2008.562	69 $\pm$ 4	-20 $\pm$ 4	17.1 $\pm$ 0.2	AO
2009.561	-33 $\pm$ 7	35 $\pm$ 7	17.35 $\pm$ 0.05	AO
2009.689	-35 $\pm$ 3	25 $\pm$ 2	17.0 $\pm$ 0.2	AO
2010.342	-57.0 $\pm$ 0.5	-33 $\pm$ 1	17.6 $\pm$ 0.2	AO
2010.511	-57 $\pm$ 4	-45 $\pm$ 6	17.5 $\pm$ 0.2	AO
2012.371	-37.5 $\pm$ 0.5	-126 $\pm$ 6	17.3 $\pm$ 0.1	AO

Table S2.

Summary of Galactic-Center Keck Speckle Observations & Imaging Analysis

Date Range (UT)	Fractional Year	Meas.	Frames SAA	SpH	FWHM (mas) SAA	K_{lim}[a] (mag) SAA	SpH
1995 June 10-12	1995.439	15,114	1,800	5,019	58	15.7	16.4
1996 June 26-27	1996.485	9,261	865	2,908	60	14.6	15.7
1997 May 13	1997.367	3,811	1,837	3,380	61	15.7	16.6
1998 April 2	1998.251	3,184	1,639	· · ·	62	15.1	· · ·
1998 May 14-15	1998.366	16,531	2,102	· · ·	69	15.8	· · ·
1998 July 4	1998.505	9,751	933	3,964	63	15.7	16.3
1998 Aug 4-5	1998.590	20,375	1,933	11,500	62	15.8	17.3
1998 Oct 9-11	1998.771	4,776	1,082	· · ·	56	15.7	· · ·
1999 May 2-4	1999.333	19,512	1,857	10,835	72	16.2	17.3
1999 July 24	1999.559	19,307	2,108	5,684	57	16.2	17.2
2000 May 19-20[b]	2000.381	21,492	2,492	15,800	56	15.9	17.2
2000 July 19-20[b]	2000.548	15,124	1,581	10,878	63	16.3	16.8
2000 Oct 18[b]	2000.797	2,587	1,517	· · ·	60	15.0	· · ·
2001 May 7-9	2001.351	11,343	1,994	6,136	56	16.7	16.9
2001 July 28-29	2001.572	15,920	1,695	13,416	57	15.9	17.4
2002 April 23-24[b]	2002.309	16,130	1,958	5,777	67	15.9	16.2
2002 May 23-29[b]	2002.391	18,338	1,443	12,710	60	15.7	17.0
2002 July 19-20[b]	2002.547	8,878	1,118	6867	63	16.2	17.0
2003 April 21-22	2003.303	14,475	1,841	9,463	62	15.8	16.9
2003 July 22-23	2003.554	6,948	1,703	3,535	65	16.1	17.0
2003 Sept 7-8	2003.682	9,799	1,723	· · ·	65	16.0	· · ·
2004 April 29-30	2004.327	20,140	1,423	9,518	63	16.0	17.7
2004 July 25-26	2004.564	14,440	2,161	8,593	61	15.9	17.3
2004 August 29	2004.660	3,040	1,301	· · ·	60	15.9	· · ·
2005 April 24-25[b]	2005.312	15,770	1,679	12,992	60	15.9	17.1
2005 July 26-27	2005.566	14,820	1,331	· · ·	62	15.5	· · ·

[a]K_{lim} is the magnitude at which the cummulative distribution function of the observed K magnitudes reaches 95% of the total sample size.

[b]These epochs have been analysed with an improved version of the holography algorithm that employs a larger Field-Of-View and better masking/centroiding of the reference sources.

Table S3.

Summary of Galactic Center Keck Adaptive Optics Observations & Imaging Analysis

Date Range (UT)	Fractional Year	Frames Meas.	Frames Used	Coadd $\times$ T_{exp} (sec)	FWHM (mas)	Strehl	K_{lim}[c] mag
2004 July 26	2004.567	12	12	50×0.181	60	0.29	16.2
2005 June 30	2005.495	10	10	$5 \times 7.2/11.9$[f]	61	0.27	16.7
2005 July 30-31	2005.580	66	31	10×2.8	57	0.20	19.5
2006 May 3	2006.336	153	107	10×2.8	58	0.24	19.7
2006 June 20-21	2006.470	295	156	10×2.8	57	0.30	20.0
2006 July 17	2006.541	70	64	10×2.8	58	0.28	19.7
2007 May 17	2007.374	103	76	10×2.8	58	0.30	19.8
2007 Aug 10-12	2007.612	142	78	10×2.8	57	0.24	19.5
2008 May 15[a]	2008.371	138	134	10×2.8	54	0.25	19.8
2008 July 24	2008.562	179	104	10×2.8	58	0.29	20.0
2009 May 1-4	2009.340	311	149	10×2.8	57	0.29	19.3
2009 July 24	2009.561	146	75	10×2.8	61	0.21	19.7
2009 Sept 9	2009.689	55	43	10×2.8	61	0.26	19.5
2010 May 4-5	2010.342	219	158	10×2.8	63	0.23	19.7
2010 July 6	2010.511	136	117	10×2.8	61	0.31	19.8
2010 Aug 15	2010.620	143	127	10×2.8	60	0.21	19.6
2011 May 27	2011.401	164	114	10×2.8	66	0.19	19.2
2011 July 18[a]	2011.543	212	167	10×2.8	59	0.21	19.6
2011 Aug 23	2011.642	218	196	10×2.8	59	0.28	19.9
2012 May 15 & 18	2012.371	290	201	10×2.8	59	0.25	19.8

[a]In contrast to other epochs, a natural guide star, instead of a laser guide star, was used for either all (2011 July) or part of the observations (2008 May; NGS 22 used and LGS 112 used) during this epoch, due to the unavailability of the laser.

[c]K_{lim} is the magnitude at which the cummulative distribtuion function of the observed K magnitudes reaches 95% of the total sample size.

[f] Half of the images were taken using a narrow band CO filter, with the shorter exposure time, and the other half using a narrow band K_{cont} filter, with the longer exposure time.

Table S4.

S0-2's orbit[a]

Parameter [Unit]	Value
Period [years]	16.17 ± 0.15
Time of Closest Approach [year]	2002.346 ± 0.01
Eccentricity	0.898 ± 0.005
Inclination [degrees]	132.8 ± 1
Angle to Periapse [degrees]	65.2 ± 1
Position Angle of the Ascending Node [degrees]	225.7 ± 0.8
Mass [10^6 M_{Sun}]	4.1 ± 0.4
Distance [kpc]	7.7 ± 0.4
X_0[b,c] (orbit's focal point) [mas]	$0.1 \pm 1.0 \pm 0.8$[d]
Y_0[b] (orbit's focal point) [mas]	$-6.6 \pm 1.4 \pm 1.1$[d]
X velocity [mas/year]	-0.19 ± 0.1
Y velocity [mas/year]	0.57 ± 0.2
Z velocity [km/s]	15 ± 20

[a]The best fit has a χ^2 of 73.34 with 96 degrees-of-freedom.

[b]The reference time for the position is 2000.0.

[c]X is defined to be positive to the east.

[d]The second error marks the uncertainty in the procedure of constructing an infrared reference frame. It has been calculated from Table 5 in Yelda et al. (35).

Table S5.

Orbital elements for S0-104[a]

Parameter [Unit]	Value
Period [years]	80 ± 35
Time of Closest Approach [year]	2009.5 ± 0.1
Eccentricity	$0.988^{+0.007}_{-0.025}$
Inclination [degrees]	87.5 ± 1
Angle to Periapse [degrees]	250 ± 1
Position Angle of the Ascending Node [degrees]	144 ± 1.5

[a]The best fit has a χ^2 of 22.44 with 14 degrees-of-freedom.

References and Notes

1. A. Eckart, R. Genzel, *Mon. Not. R. Astron. Soc.* **284**, 576 (1997).

2. A. M. Ghez, B. L. Klein, M. Morris, E. E. Becklin, High proper-motion stars in the vicinity of Sagittarius A*: Evidence for a supermassive black hole at the center of our galaxy. *Astrophys. J.* **509**, 678 (1998). doi:10.1086/306528

3. A. M. Ghez, M. Morris, E. E. Becklin, A. Tanner, T. Kremenek, The accelerations of stars orbiting the Milky Way's central black hole. *Nature* **407**, 349 (2000). doi:10.1038/35030032 Medline

4. A. Eckart, R. Genzel, T. Ott, R. Schödel, Stellar orbits near Sagittarius A. *Mon. Not. R. Astron. Soc.* **331**, 917 (2002). doi:10.1046/j.1365-8711.2002.05237.x

5. R. Schödel *et al.*, A star in a 15.2-year orbit around the supermassive black hole at the centre of the Milky Way. *Nature* **419**, 694 (2002). doi:10.1038/nature01121 Medline

6. A. M. Ghez *et al.*, The first measurement of spectral lines in a short-period star bound to the galaxy's central black hole: A paradox of youth. *Astrophys. J.* **586**, L127 (2003). doi:10.1086/374804

7. A. M. Ghez *et al.*, Measuring distance and properties of the Milky Way's central supermassive black hole with stellar orbits. *Astrophys. J.* **689**, 1044 (2008). doi:10.1086/592738

8. S. Gillessen *et al.*, Monitoring stellar orbits around the massive black hole in the galactic center. *Astrophys. J.* **692**, 1075 (2009). doi:10.1088/0004-637X/692/2/1075

9. S. Gillessen *et al.*, The orbit of the star S2 around Sgr A* from Very Large Telescope and Keck data. *Astrophys. J.* **707**, L114 (2009). doi:10.1088/0004-637X/707/2/L114

10. S0-102 might be identical to the star labeled S55 in (*8*), for which only linear motion is reported there.

11. K. Matthews, B. T. Soifer, in *Astronomy with Infrared Arrays: The Next Generation*, I. McLean, Ed. (Kluwer, Netherlands, 1994), pp. 239–246.

12. K. Matthews, A. M. Ghez, A. J. Weinberger, G. Neugebauer, The first diffraction-limited images from the W. M. Keck telescope. *Publ. Astron. Soc. Pac.* **108**, 615 (1996). doi:10.1086/133773

13. A. M. Ghez *et al.*, Stellar orbits around the galactic center black hole. *Astrophys. J.* **620**, 744 (2005). doi:10.1086/427175

14. J. R. Lu *et al.*, A disk of young stars at the galactic center as determined by individual stellar orbits. *Astrophys. J.* **690**, 1463 (2009). doi:10.1088/0004-637X/690/2/1463

15. A. M. Ghez *et al.*, The first laser guide star adaptive optics observations of the galactic center: Sgr A*'s infrared color and the extended red emission in its vicinity. *Astrophys. J.* **635**, 1087 (2005). doi:10.1086/497576

16. S. D. Hornstein *et al.*, A constant spectral index for Sagittarius A* during infrared/x-ray intensity variations. *Astrophys. J.* **667**, 900 (2007). doi:10.1086/520762

17. A detailed description of the methods is available as supplementary materials on *Science* Online.

18. E. Diolaiti *et al.*, Analysis of isoplanatic high resolution stellar fields by the StarFinder code. *Astron. Astrophys. Suppl. Ser.* **147**, 335 (2000). doi:10.1051/aas:2000305

19. The distance to the black hole and its line-of-sight velocity cannot be determined, because a measurement of the star's radial velocity is needed for this. S0-102 is currently just beyond the spectroscopic limit.

20. S0-104 is a previously unknown detected star; its orbital motion is presented in the supplementary materials on *Science* Online.

21. W. I. Hartkopf, B. D. Mason, E. Worley, *Astron. J.* **122**, 3471 (2001).

22. C. Will, *Living Rev. Relativity* **9**, 3 (2006); available at www.livingreviews.org/lrr-2006-3.

23. The strength of the gravitational field we quote here relates to the interbody potential and therefore orbital velocities. However, we want to note that the strong-field internal gravity of the neutron stars could leave imprints on the orbital motion.

24. S. Zucker, T. Alexander, S. Gillessen, F. Eisenhauer, R. Genzel, Probing post-Newtonian physics near the galactic black hole with stellar redshift measurements. *Astrophys. J.* **639**, L21 (2006). doi:10.1086/501436

25. R. AngŽlil, P. Saha. *Astrophys. J.* **734**, L19 (2011).

26. M. Jaroszynski, *Acta Astronomica* **48**, 653 (1998).

27. G. F. Rubilar, A. Eckart, Periastron shifts of stellar orbits near the Galactic Center. *Astron. Astrophys.* **374**, 95 (2001). doi:10.1051/0004-6361:20010640

28. N. N. Weinberg, M. Milosavljevic, A. M. Ghez, Stellar Dynamics at the Galactic Center with an Extremely Large Telescope. *Astrophys. J.* **622**, 878 (2005). doi:10.1086/428079

29. C. M. Will, Testing the general relativistic "no-hair" theorems using the galactic center black hole Sagittarius A. *Astrophys. J.* **674**, L25 (2008). doi:10.1086/528847

30. R. AngŽlil, P. Saha, D. Merritt, *Astrophys. J.* **720**, 1303 (2010).

31. D. Merritt, T. Alexander, S. Mikkola, C. M. Will, Testing properties of the Galactic center black hole using stellar orbits. *Phys. Rev. D Part. Fields Gravit. Cosmol.* **81**, 062002 (2010). doi:10.1103/PhysRevD.81.062002

32. A. Gualandris, S. Gillessen, D. Merritt, The galactic centre star S2 as a dynamical probe for intermediate-mass black holes. *Mon. Not. R. Astron. Soc.* **409**, 1146 (2010). doi:10.1111/j.1365-2966.2010.17373.x

33. M. R. Morris, Massive star formation near the Galactic center and the fate of the stellar remnants. *Astrophys. J.* **408**, 496 (1993). doi:10.1086/172607

34. J. Miralda-Escude, A. Gould, A cluster of black holes at the galactic center. *Astrophys. J.* **545**, 847 (2000). doi:10.1086/317837

35. S. Yelda *et al.*, Improving galactic center astrometry by reducing the effects of geometric distortion. *Astrophys. J.* **725**, 331 (2010). doi:10.1088/0004-637X/725/1/331

36. W. I. Clarkson *et al.*, Proper motions of the arches cluster with Keck laser guide star adaptive optics: The first kinematic mass measurement of the arches. *Astrophys. J.* **751**, 132 (2012). doi:10.1088/0004-637X/751/2/132

37. S. D. Hornstein *et al*., Limits on the short-term variability of Sagittarius A* in the near-infrared. *Astrophys. J.* **577**, L9 (2002). [doi:10.1086/344098](doi:10.1086/344098)

38. S. D. Hornstein, thesis, University of California, Los Angeles (2007).

39. R. Schödel *et al*., Holographic imaging of crowded fields: An effective poor man's adaptive optics system (2012); available at http://arxiv.org/abs/1110.2261v3.

40. J. C. Christou, S. T. Ridgway, D. F. Buscher, C. A. Haniff, D. W. McCarthy Jr., *ASP Conf. Ser.* **14**, 133 (1991).

41. J. Primot, G. Rousset, J. C. Fontanella, Deconvolution from wave-front sensing: A new technique for compensating turbulence-degraded images. *J. Opt. Soc. Am. A* **7**, 1598 (1990). doi:10.1364/JOSAA.7.001598

42. M. G. Petr, V. Coude Du Foresto, S. V. W. Beckwith, A. Richichi, M. J. McCaughrean, Binary stars in the Orion trapezium cluster core. *Astrophys. J.* **500**, 825 (1998). [doi:10.1086/305751](doi:10.1086/305751)